The Role of Surface Wettability on the Growth of Vapour Bubbles

International Journal of Heat and Mass Transfer 217 (2023) 124657

Contents lists available at ScienceDirect

International Journal of Heat and Mass Transfer

journal homepage: www.elsevier.com/locate/ijhmt

The role of surface wettability on the growth of vapour bubbles

Patrick Sullivan [a,*], Duncan Dockar [a], Ryan Enright [b], Matthew K. Borg [a], Rohit Pillai [a]

[a] Institute for Multiscale Thermofluids, School of Engineering, University of Edinburgh, Edinburgh, EH9 3FB, Scotland, UK
[b] SEGUENTE Inc., 1333 Gateway Dr., Suite 1002, Melbourne, 32901, FL, USA

ARTICLE INFO

Dataset link: https://doi.org/10.7488/ds/7511

Keywords:
Bubble growth
Molecular dynamics
Wettability

ABSTRACT

The formation of heterogeneous vapour bubbles is widely studied due to its importance to two-phase thermal management systems, ultrasonic cleaning, and turbomachinery performance. However, the role that the surface plays in determining the growth of a bubble is still poorly understood. Currently, theoretical understanding of heterogeneous vapour bubble growth is limited to hemispherical bubbles or completely spherical bubbles next to a surface. We have previously developed an inertio-thermal model to accurately predict how heat transfer from the surrounding fluid affects *homogeneous* vapour bubble growth from the nanoscale to the macroscale (Sullivan et al. *J. Fluid Mech.* 948(A55):1-15, 2022). By accounting for the presence of the surface and its wettability on both the geometry of the bubble and on the available thermal energy in the surrounding fluid, we extend our model to capture *heterogeneous* vapour bubble growth. Using molecular simulations, we show not only how the strength of fluid-solid interaction affects the growth rate, but also how the formation of an adsorbed fluid layer under the bubble on lyophilic surfaces plays a vital role in determining the bubble shape and subsequent dynamics. These insights have potential to improve the performance of systems involving a change of phase from liquid to vapour by better understanding the role of surface wettability on this process.

1. Introduction

Vapour bubble formation has been attributed as the driving factor behind natural phenomena, such as geyser formation and volcanic eruptions [1]. Similarly, the explosive failure of pressurised containers and wear of turbomachinery caused by cavitation bubbles, highlight the deleterious effects of vapour bubbles on industrial processes [2]. The high heat fluxes dissipated from surfaces during bubble formation and growth have seen flow and pool boiling attracting significant interest for use in (opto)electronic thermal management systems [3].

Early studies on the growth rate of homogeneous vapour bubbles focused on analysing either the effects of limiting inertia [4] or heat transfer [5]. The inertial growth of such spherical bubbles is described by the Rayleigh–Plesset (RP) equation, which balances the driving forces from the pressure difference across the bubble's interface with the inertia of the liquid phase [4]. The RP equation includes the effects of capillarity and viscosity on the pressure difference, which are most relevant for small bubbles [6], and has been extended to include the effects of mass transfer at the liquid-vapour interface [7]. Where heat transfer is the dominant factor controlling bubble growth rate, Plesset and Zwick [5] considered the energy balance at the bubble interface, balancing the latent heat required to grow the bubble with the heat available through conduction to the interface. These two limiting cases of inertial and thermal bubble growth were combined by Mikic et al. [8], who interpolated between the inertial limiting velocity of the RP equation and the thermal limiting velocity of the Plesset–Zwick solution, showing good agreement with a wide range of bubble growth data [1,9,10]. Recently, we have developed a more accurate approach by including the changing inertial growth (rather than using a constant inertial limiting velocity) in our *inertio-thermal* bubble growth models, showing improved agreement in the early stages of bubble growth across experiments and simulations [11].

While these models are useful in the idealised case of perfectly-spherical bubbles growing in an infinite medium, in practice, bubbles typically form at a solid surface, where the barrier to nucleation is reduced [12]. This significantly changes the physics controlling the growth rate, as the presence of the solid surface alters the diffusive heat transfer in the liquid surrounding the bubble [13]. To simplify the analysis of heterogeneous bubble growth, either spherical or hemispherical bubbles on a solid surface are typically analysed. Mikic et al. [8] proposed a model for the growth of spherical bubbles at a wall by using an error function solution to capture the non-uniform temperature

* Corresponding author.
E-mail addresses: psulliva@tcd.ie, Patrick.Sullivan@ed.ac.uk (P. Sullivan).

https://doi.org/10.1016/j.ijheatmasstransfer.2023.124657
Received 15 May 2023; Received in revised form 1 August 2023; Accepted 28 August 2023
Available online 11 September 2023

field close to a heated surface. However, the model did not account for the changes in diffusive heat transfer that arise in the surrounding liquid when a bubble grows on a wall, predicting identical results to their homogeneous bubble growth model in the case of a uniformly heated fluid. Indeed, they show a disagreement of a factor of two with experimental results. The altered thermal diffusive behaviour near the wall resembles the case of the growth of gas bubbles by species diffusion analysed by Enríquez et al. [13], who showed how the solid surface halved the growth rate of spherical bubbles on a surface when compared to a homogeneous bubble growth theory. The approach of Enríquez et al. [13] has not yet been adapted to analyse bubble growth driven by the unique thermal diffusion field from the surrounding liquid rather than species diffusion and has not been extended to model the growth of partially wetting bubbles, only considering the case of spherical bubbles touching the surface at a single point.

In the context of partially wetting bubbles, much of the existing literature has focused on the heat transfer into the bubble from the surface. Cooper and Lloyd [14] developed a model for hemispherical bubble growth on a heated surface driven entirely by evaporation from the liquid microlayer under the bubble, but neglected heat transfer from the bulk fluid. Later, van Stralen et al. [15] incorporated heat transfer through the bubble cap, in addition to the microlayer, using a laminar boundary layer heat transfer approximation. However, their model requires knowledge of the time the bubble will take to leave the surface due to buoyancy, and therefore cannot be used to predict bubble growth *a priori*. The models by Cooper and Lloyd [14] and van Stralen et al. [15] additionally neglect the effect of the contact angle on bubble growth rate, only modelling hemispherical bubble growth. Despite the significance of wettability in bubble nucleation [12] and departure from the surface [3], its effect on growth rate remains unexplored.

In addition to theoretical modelling, a wide range of experimental and numerical investigations have been performed on heterogeneous vapour bubble dynamics, typically focused on the departure of bubbles from heated surfaces [16–20]. In these cases, surface wettability is typically measured using the contact angle of liquid droplets, however, Ardron and Giustini [21] have recently shown that the presence of a nanoscale adsorbed layer underneath vapour bubbles alters the free energy balance that determines the shape of the bubble, indicating that contact angle measurements using droplets cannot always accurately predict the contact angle of vapour bubbles. Note that this nanoscale adsorbed layer is only a few molecules thick, and is distinct from the micron-sized liquid micro-layer observed in pool boiling phenomena [22]. To avoid confusion between the two, it is often referred to as a non-evaporating layer (NEL) [23]. Previous continuum-based numerical investigations into the influence of surface wettability on vapour bubble dynamics were not capable of capturing the adsorbed layer, even after accounting for the changes to average near wall density [24]. Molecular dynamics (MD) simulations in contrast have been able to capture adsorbed layers underneath vapour bubbles [25,26], making MD a unique tool for studying the complete physics of surface wettability on nanoscale heterogeneous vapour bubble growth.

In summary, our understanding of heterogeneous bubble growth is currently limited to idealised approximations of bubble shapes and neglect the effects of the surface on the geometry of the bubble and diffusive heat transfer in the bulk liquid. It has been shown in literature that surface wettability plays a significant role in the formation and detachment of vapour bubbles, but there is currently little understanding of its effect on bubble growth, particularly in the early stages, when buoyancy forces are less relevant. Using MD, in this work we perform heterogeneous bubble growth simulations of nanoscale vapour bubbles. The bubble's interface is also modified in these simulations through simple changes in surface wettability to investigate its influence on the diffusive heat transfer during bubble growth. We present a new analytical model for the growth of heterogeneous vapour bubbles in a uniformly heated liquid, which extends our recently developed inertio-thermal model [11] for homogeneous bubble growth. We compare the predictions of our model to our MD results, showing good agreement, provided that the bubble shape can be accurately determined and the system inertia can be approximated with spherical symmetry.

2. Development of theoretical model

Spherical vapour bubble growth in an infinite medium is described by the RP equation, which balances the pressure difference across the bubble interface with the inertial resistance to growth. For the case of a Newtonian fluid, neglecting the effects of mass transfer at the bubble interface, the RP equation is given as:

$$R\ddot{R} + \frac{3}{2}\dot{R}^2 = \frac{1}{\rho_l}\left(P_v - P_\infty - \frac{2\gamma}{R} - \frac{4\mu\dot{R}}{R}\right), \tag{1}$$

where R is the radius of the bubble and dots are used to represent the time derivative. The liquid density, surface tension, and dynamic viscosity are given by ρ_l, γ, and μ, respectively. The terms on the left hand side of the equation represent the liquid phase's inertia, while the right hand side accounts for the vapour pressure inside the bubble P_v, the fluid far field pressure P_∞, Laplace pressure $2\gamma/R$, and viscous pressure $4\mu\dot{R}/R$. From this expression, the maximum growth velocity of a bubble can be shown to be [2]:

$$\dot{R}_{\mathrm{RP,max}} = \sqrt{\frac{2\Delta P}{3\rho_l}}, \tag{2}$$

where $\Delta P = P_v - P_\infty$.

As an isolated bubble grows, maintaining the pressure inside the bubble requires evaporation of the surrounding liquid. The latent heat requirements associated with this vapour formation must be provided by sensible heat conduction from the bulk liquid. We can write the energy balance at the interface as:

$$\rho_v h_{lv} \dot{V}_{sp} = A_{sp} q'', \tag{3}$$

where ρ_v and h_{lv} represent the vapour density and latent heat of evaporation, respectively, and $\dot{V}_{sp}$ is the rate of change of volume of the bubble. The heat flux is given as q'' across the interface of area A_{sp}. Solutions to Eq. (3) have been found for spherical bubbles by Scriven [27] and Plesset and Zwick [5], who solved for the heat flux using a thin thermal boundary layer approximation. Mikic et al. [8] interpolated between the inertial limit of Eq. (2) and the thermal limit of Plesset and Zwick [5], producing the MRG model for the radial velocity of a bubble, given as:

$$\dot{R}_{\mathrm{MRG}} = \dot{R}_{\mathrm{RP,max}}\left[\sqrt{\frac{\dot{R}^2_{\mathrm{RP,max}}}{B^2}t + 1} - \sqrt{\frac{\dot{R}^2_{\mathrm{RP,max}}}{B^2}t}\right], \tag{4}$$

where $B = Ja\sqrt{12\alpha/\pi}$. Here, $\alpha = k/\rho_l c_p$ is the thermal diffusivity of the liquid, k is the thermal conductivity, and c_p is the specific heat capacity. The Jakob number Ja, is the ratio of sensible heat to latent heat, given by $Ja = \rho_l c_p \Delta T_0/\rho_v h_{lv}$, where ΔT_0 is the initial liquid superheat, i.e. the difference between the temperature of the fluid and the saturation temperature.

Recently, we developed a new class of inertio-thermal (IT) models which accurately tracks homogeneous bubble growth from the nanoscale to the macroscale [11]. A simplified IT model was shown to be accurate when the timescale of the acceleration of the bubble is less than the timescale at which thermal effects become dominant in determining the bubble growth rate [11]. This simplified IT model predicts the radial velocity of an initially static vapour bubble using a combination of the radial velocities predicted by solving the RP equation $\dot{R}_{\mathrm{RP}}$ (Eq. (1)) and the MRG model $\dot{R}_{\mathrm{MRG}}$ (Eq. (4)):

$$\dot{R}_{\mathrm{IT}} = \frac{\dot{R}_{\mathrm{RP}}\dot{R}_{\mathrm{MRG}}}{\dot{R}_{\mathrm{RP,max}}}. \tag{5}$$

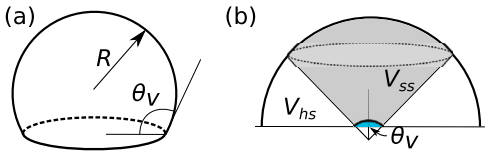

Fig. 1. (a) Example of a spherical cap, defined by the bubble radius of curvature R and contact angle θ_v. (b) Comparison of the volume occupied by a hemisphere surrounding the heterogeneous bubble and the spherical sector of cone angle θ_v, shaded in gray. The vapour bubble (highlighted in blue) has the same contact angle as the cone angle that extends from its centre of curvature. (For interpretation of the colours in the figure(s), the reader is referred to the web version of this article.)

In this paper, we will adapt this solution for the case of a heterogeneous bubble on an adiabatic surface. This allows us to neglect the effects of heat transfer from the surface, and isolate the role of wettability in modifying diffusive heat transfer from the bulk liquid. This is achieved by modifying the terms of Eq. (3) to account for the altered geometry of the bubble. We will assume the bubble takes the shape of a spherical cap on the surface, shown in Fig. 1(a), as this is the shape that minimises the interfacial free energy [28,29], which is particularly relevant to bubbles close to the critical radius for nucleation where capillary effects dominate. In the cases investigated here, the validity of this approximation is quantified through the Weber number $We = \rho_l \dot{R}_{\mathrm{RP,max}} R_0/\gamma$, where R_0 is the initial radius of the bubble, and capillary number $Ca = \mu \dot{R}_{\mathrm{RP,max}}/\gamma$, which represent the ratio of inertial to capillary forces and viscous to capillary forces, respectively. As both quantities are small, i.e., $We, Ca \approx 0.1$ capillary forces are the dominant factor in determining the shape of the bubbles. The volume of a spherical cap V_{sc} can be expressed in terms of the volume of the sphere of equal radius as:

$$\frac{V_{sc}}{V_{sp}} = \frac{\left(2+\cos\theta_v\right)\left(1-\cos\theta_v\right)^2}{4}, \tag{6}$$

where θ_v is the vapour side contact angle of the bubble. Similarly, the surface area of the spherical cap A_{sc} can be expressed in terms of the area of the sphere A_{sp} as:

$$\frac{A_{sc}}{A_{sp}} = \frac{\left(1-\cos\theta_v\right)}{2}. \tag{7}$$

Taking the ratio of these two scaling factors, i.e. the ratio of the volume scaling to surface area scaling of a spherical cap, gives:

$$\psi(\theta_v) = \frac{V_{sc}}{V_{sp}}\left(\frac{A_{sc}}{A_{sp}}\right)^{-1} = \frac{1}{2}\left(2+\cos\theta_v\right)\left(1-\cos\theta_v\right). \tag{8}$$

The energy balance from Eq. (3) can now be written for a spherical cap in terms of the sphere with the same radius and the factor ψ as:

$$\psi(\theta_v)\rho_v h_{lv} \dot{V}_{sp} = A_{sp} q''. \tag{9}$$

While Eq. (9) accounts for the geometrical differences in heat transfer at the bubble interface, it does not account for the change in available thermal energy due to the presence of the adiabatic wall. To account for this, we assume that the available thermal energy is contained in a hemisphere around the bubble. The ratio of the volume of this hemisphere V_{hs} to the volume of the spherical sector V_{ss} of the same radius with a cone angle matching the bubble's contact angle gives a comparison of the difference in thermal energy surrounding the heterogeneous bubble compared to a homogeneous bubble of the same radius. This is illustrated in Fig. 1(b). This gives a further scaling factor on the heat flux of:

$$\frac{V_{ss}}{V_{hs}} = 1-\cos\theta_v. \tag{10}$$

Dividing the scaling factor from Eq. (8) by the energy scaling factor in Eq. (10), an overall scaling factor for heterogeneous bubble growth $H(\theta_v)$ is obtained:

$$H(\theta_v) = \frac{1}{2}\left(2+\cos\theta_v\right). \tag{11}$$

Taking the liquid and vapour angles to be complementary $\theta_l = 180° - \theta_v$, the heterogeneous scaling factor can be expressed in terms of θ_l as:

$$H(\theta_l) = \frac{1}{2}\left(2-\cos\theta_l\right). \tag{12}$$

We can now express the growth rate of heterogeneous bubbles in terms of the equivalent homogeneous bubble growth rate $\dot{R}_{sp}$ as:

$$\dot{R}(\theta_l) = H(\theta_l)\dot{R}_{sp} = \frac{1}{2}\left(2-\cos\theta_l\right)\dot{R}_{sp}. \tag{13}$$

This new theoretical model allows us to predict the growth of heterogeneous bubbles by adapting homogeneous analyses. We can use this to express a heterogeneous inertio-thermal (HIT) model as:

$$\dot{R}_{\mathrm{HIT}}(\theta_l) = H(\theta_l)\dot{R}_{\mathrm{IT}}, \tag{14}$$

where we will refer to $H(\theta_l)$ as the HIT factor that relates the homogeneous growth prediction ($\dot{R}_{\mathrm{IT}}$) to the heterogeneous one ($\dot{R}_{\mathrm{HIT}}$).

3. Simulation methodology

Molecular dynamics (MD) simulations were performed to measure the growth of nanoscale vapour bubbles, using the open source software LAMMPS [30]. The interactions between the molecules were calculated using the Lennard–Jones (LJ) potential:

$$U(r_{ij}) = 4\varepsilon_{ij}\left[\left(\frac{\sigma_{ij}}{r_{ij}}\right)^{12} - \left(\frac{\sigma_{ij}}{r_{ij}}\right)^{6}\right], \tag{15}$$

where σ is the characteristic length scale, ε is the potential well depth, and r is the distance between two molecules denoted by the subscripts i and j. The fluid (subscript f) interaction parameters used in these simulations are $\sigma_f = 0.34$ nm and $\varepsilon_f = 0.2392$ kcal/mol, respectively, which were chosen to model argon [25]. The solid (subscript s) potential parameters used were $\sigma_s = 0.247$ nm and $\varepsilon_s = 15.9743$ kcal/mol, chosen to model platinum [31]. The LJ potential is truncated for values of $r > r_{\mathrm{cut}}$, where $r_{\mathrm{cut}} = 1.3$ nm. The simulations are performed with a timestep of 5 fs.

To investigate the effect of surface wettability, we adjust the molecular potential using the model of Nagayama and Cheng [32]. This model is based on the Lorentz–Berthelot mixing rules which predict the effective length and energy scales for the solid-fluid interaction [31], σ_{sf} and ε_{sf}, respectively, in terms of the solid and fluid values to be:

$$\sigma_{sf} = b^{1/6}\frac{\sigma_s+\sigma_f}{2}, \tag{16}$$

$$\varepsilon_{sf} = ab^2\sqrt{\varepsilon_s\varepsilon_f}. \tag{17}$$

Their model [32] further incorporates the modifications made by Din and Michaelides [33] to the magnitude of the potential as well as by Barrat and Bocquet [34] to the attractive portion of the potential. Two new non-dimensional scaling factors are introduced; the factor a scales the magnitude of the potential, while the factor b adjusts the balance of attractive to repulsive components.

To achieve a range of partial wetting cases, a fixed value of $a = 0.14$ was used [35], allowing for wettability to be controlled by b alone [34]. The values of b used, and the corresponding contact angles, are given in Table 1. In addition to these partially wetting cases, a completely wetting case with $\theta_l = 0°$ was performed. This was achieved by using the fluid-fluid values of σ and ε for the solid-fluid interactions (i.e. $\sigma_{sf} = \sigma_f = 0.34$ nm and $\varepsilon_{sf} = \varepsilon_f = 0.2392$ kcal/mol).

The system setup used in the MD simulation is shown in Fig. 2. A liquid slab was created using the software package Packmol [36], with the

Table 1
LJ scaling factors for varying wettability surfaces with approximate droplet contact angles.

b	θ_l [°]
0.9	10
0.7	40
0.65	55
0.6	70
0.5	95
0.4	120
0.3	150

dimensions of the slab chosen depending on the expected contact angle. The dimensions ranged from a height of 45 nm and length of 60 nm for the most wetting cases, to a height of 20 nm and length of 70 nm for the least wetting cases. The number of argon molecules N was chosen to be slightly lower than the saturation density, creating a supersaturated liquid. This value ranged from 5×10^5 to 1.5×10^6 molecules depending on the case being tested. This liquid slab was contained between two rigid FCC walls, which are used to maintain the fluid pressure during the bubble's growth. During the simulation, the lower wall is kept fixed in place, while the upper wall, which we call the piston, is allowed to translate in the normal direction after fluid equilibration to allow for bubble expansion. The other boundaries of the domain are periodic.

The liquid is initially equilibrated (with both surfaces fixed) in the NVT ensemble until the potential energy reached a steady value. The piston is then released to apply the required pressure $P_\infty = 0.1$ MPa, through a constant force F, applied to each atom. This force is given by $F = P_\infty A_P / N_P$, where A_P is the surface area of the piston, and N_P is the number of piston atoms. During this stage, a damping constant of $c = 7$ fNs/m was applied to the motion of each piston molecule to prevent excessive oscillations, which could lead to cavitation bubbles forming in the liquid. The system was equilibrated again in the NVT ensemble until the piston reached a steady position, at which point the damping constant was removed.

At this point in the simulation setup, a spherical cap of molecules with a specified radius was removed from the liquid next to the stationary surface. The cap's radius of curvature was chosen to be above the critical radius for the specified temperature and pressure and the contact angle of the cap was set to match the expected wettability of the surface, allowing for control over the size and shape of the bubble for each investigation. A smaller number of vapour molecules were then inserted into this void, with the number of molecules set to match the saturated vapour density. This system was then run with the fluid in the NVT ensemble for 1000 timesteps to equilibrate the bubble, preventing any cavitation bubbles from forming in the system, and the setup was considered to be fully equilibrated at this point. The production simulations could then be performed with the fluid in the NVE ensemble. The lower wall atoms were fixed in position during this time, which was equivalent to setting an adiabatic surface, and prevented any heat transfer to the fluid. These simulations were run for a total of 200,000 timesteps, corresponding to a duration of 1 ns.

The vapour bubbles were detected and their size measured using the same technique as described in our previous work [11]. A non-interacting grid was overlayed onto the simulation domain. The coordination number of these grid points in relation to surrounding MD molecules was computed to determine if these grid points were located in liquid or vapour regions. A threshold of 15 molecules or greater within a radius of 1.3 nm was chosen to determine if a grid point was in a liquid region. This value was scaled by the appropriate volumetric factor for grid points near the solid surface. By calculating the number of grid points in vapour regions, the bubble volume could be measured. An example of a measured bubble profile is shown in Fig. 2.

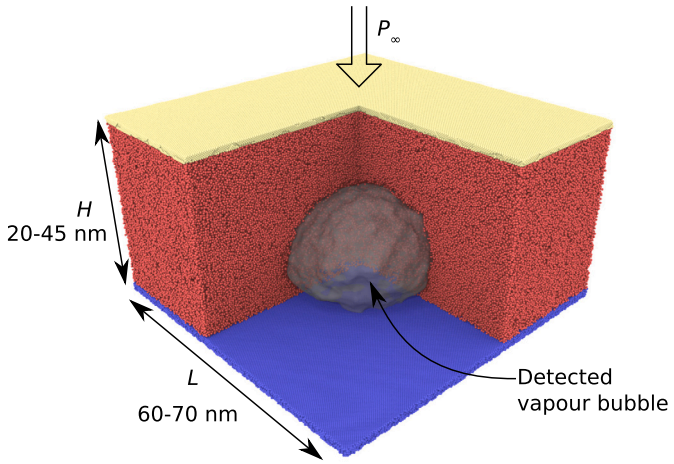

Fig. 2. Sample MD simulation setup with detected bubble highlighted (coloured grey). The simulation domain length L and height H are chosen based on the expected contact angle of the bubble. The pressure of the system is controlled by applying a constant force on the piston atoms (coloured yellow). Some of the fluid and piston atoms are not shown to improve the view of the bubble.

4. Results and discussion

4.1. Comparison of MD results to HIT model

In order to test the accuracy of the HIT model, we compare the predicted values of $H(\theta_l)$ to the values measured from MD simulations. Taking the radial velocities measured from MD as the heterogeneous values and the predictions of the homogeneous IT model at the same conditions of temperature, pressure, and initial radius, as the homogeneous values, we can rewrite Eq. (14) to give the MD measured value $H_{\mathrm{MD}}(\theta_l)$ as:

$$H_{\mathrm{MD}}(\theta_l) = \frac{\dot{R}_{\mathrm{MD}}(\theta_l)}{\dot{R}_{\mathrm{IT}}}, \tag{18}$$

where $\dot{R}_{\mathrm{MD}}(\theta_l)$ is the heterogeneous bubble radial velocity measured from MD on a surface with a droplet contact angle of θ_l, and $\dot{R}_{\mathrm{IT}}$ is the growth rate predicted from the homogeneous IT model.

Fig. 3 shows the measured profile of a growing vapour bubble for $\theta_l = 70°$ alongside the IT (homogeneous) and HIT (heterogeneous) predictions. The measured values of $H_{\mathrm{MD}}(\theta_l)$ are shown in Fig. 4(a), compared to the theoretical HIT factor (Eq. (12)).

Fig. 4 illustrates the three distinct regimes depending on surface wettability. For the *neutral wetting regime* (when $-0.5 < \cos\theta_l < 0.5$), we see excellent agreement with the HIT model predictions. Compared to an equivalent homogeneous bubble, we see an increased growth rate on the less wetting surfaces and a decreased growth rate on the more wetting surfaces, matching our theoretical predictions. In the *lyophobic regime* ($\cos\theta_l < -0.5$), the bubble can no longer be described with the spherical symmetry needed to apply the Rayleigh–Plesset equation. This makes the growth rate of bubbles in our simulations become strongly dependent on the domain size and tend towards a 1D Stefan-type problem [37] (which we discuss in further detail in the SI). In the *lyophilic regime* ($\cos\theta_l > 0.5$), we see greater bubble growth rates than those predicted by the HIT model, which will be discussed in the next section.

4.2. Lyophilic regime

For highly-wetting surfaces, we see in Fig. 4(a) that the measured bubble growth rates exceed the rates predicted by the HIT model ($H(\theta_l) \approx 0.75$ once $\cos\theta_l > 0.5$). Interestingly, the HIT factor measured across these cases is independent of wettability, which can be seen in Fig. 4(a), where the measured cases approach a constant value instead of following the HIT trajectory predicted by surface wettability

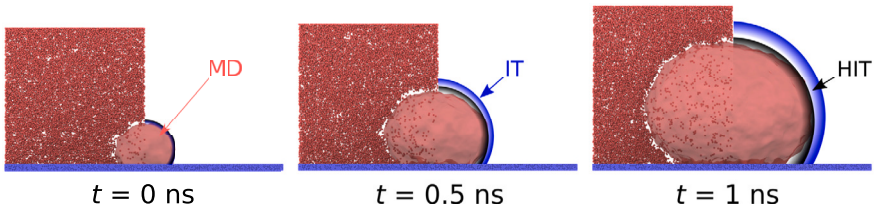

Fig. 3. Simulation snapshot segments of a growing vapour bubble for $\theta_l = 70°$. The profile measured from MD is compared to the predictions of the homogeneous IT model and the heterogeneous HIT model. Some of the liquid molecules have been removed for visualisation purposes.

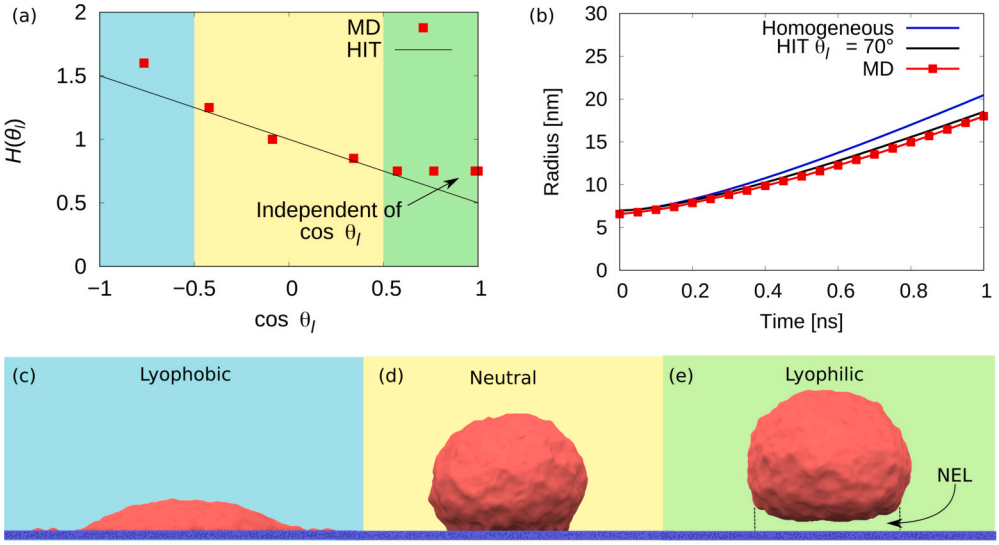

Fig. 4. (a) Measured heterogeneous scaling factors from MD simulations compared to the HIT model predictions. (b) Measured radius of vapour bubble with $\theta_l = 70°$ from MD compared to homogeneous (IT) and heterogeneous (HIT) models. Bubble profiles seen in the (c) lyophobic, (d) neutral, and (e) lyophilic regimes. A non-evaporating layer (NEL) forms underneath the bubble in the lyophilic regime. The smaller secondary bubbles visible in (c) are due to density fluctuations in the fluid near the lyophobic wall and do not affect the principle bubble's growth.

alone. This result can be explained by analysing the contact angle of the vapour bubbles on these surfaces. Fig. 5(a) shows the size dependence of the equilibrium contact angle θ_0 of the vapour bubbles measured relative to the surface for various surface wettabilities (i.e. for varying θ_l). From this plot we can see that θ_0 is independent of bubble radius for $\theta_l > 70°$ (i.e. the data appear as a flat, horizontal line), and dependent on bubble radius for $\theta_l \leq 70°$ (i.e. the data appear as tilted lines with a negative slope). When the equilibrium contact angle is independent of radius, the measured bubble contact angles θ_0 match the liquid contact angle measured from droplet simulations ($\theta_0 \approx \theta_l$). When the equilibrium contact angle is dependent on radius, the relationship between θ_0 and θ_l no longer holds. Instead, we see an interesting trend in the *limiting value of* θ_0 as the bubble radius becomes larger (and $R^{-1} \to 0$). For each of these cases, Fig. 5(a) shows that the equilibrium contact angle tends to a similar value of $\theta_0 \approx 60°$.

This behaviour can be explained by the formation of a non-evaporating layer (NEL) underneath the bubble (see Fig. 4(e)). This NEL forms due to surface adsorption of molecules once $\theta_l < 70°$, and has been shown to break the complementary nature of bubble and droplet contact angles [21]. Instead of measuring the contact angle of the bubble relative to the solid surface θ_0, we can alternatively measure the contact angle relative to the top of the NEL θ_δ (a schematic representation of the differences between these two measurements of contact angle is shown in Fig. 5(c)), again for different θ_l as shown in Fig. 5(b). The thickness of the NEL, labelled δ in Fig. 5(c), ranges from a single layer of molecules thick (≈ 0.3 nm) to over 2 nm with the thickness increasing with the surface wettability. We now see that the contact angle of the bubble becomes independent of surface wettability when a NEL forms, indicated by the collapsing of all cases onto a single line once $\theta_l < 70°$. This shows that the presence of the NEL fundamentally alters the bubble-surface interaction when compared to a bare surface. This leads to two fundamental questions: (a) by what mechanism does the NEL influence the contact angle behaviour? and (b) when and why does the NEL form?

Influence of NEL: We hypothesise that the first question, i.e. the change in the contact angle behaviour, can be attributed to the NEL changing the interfacial stress balance at the contact line. In these cases the NEL partially shields the bubble from the influence of the surface. To understand this process better, we need to quantify the variation in the interfacial stresses present in the NEL.

Using the theory of Irving and Kirkwood [38] and following the methodology from Yamaguchi et al. [39] and Nishida et al. [40], the liquid-vapour interfacial stress γ_{lv} is calculated as the integral of the difference of the normal τ_N and tangential τ_T pressure components in the direction normal to the interface from a location in the bulk liquid y_l to one in the bulk vapour y_v:

$$\gamma_{lv} = \int_{y_l}^{y_v} (\tau_N - \tau_T) dy. \tag{19}$$

Note that the precise locations of y_l and y_v (within the bulk liquid and bulk vapour, respectively) do not influence γ_{lv} as this integral is only non-zero in the interfacial region.

For the solid-liquid (γ_{sl}) and solid-vapour (γ_{sv}) interfacial stresses, it is simpler to measure the interfacial stress relative to a bare surface. In these cases, the lower bound of the integral is adjusted to be the fluid interface y_{sf} [39] with the higher bound at some location in the bulk fluid y_f. Eq. (19) is then modified in terms of the difference between the solid-fluid interfacial stress γ_{sf} and the bare surface γ_{s0} to give [39]:

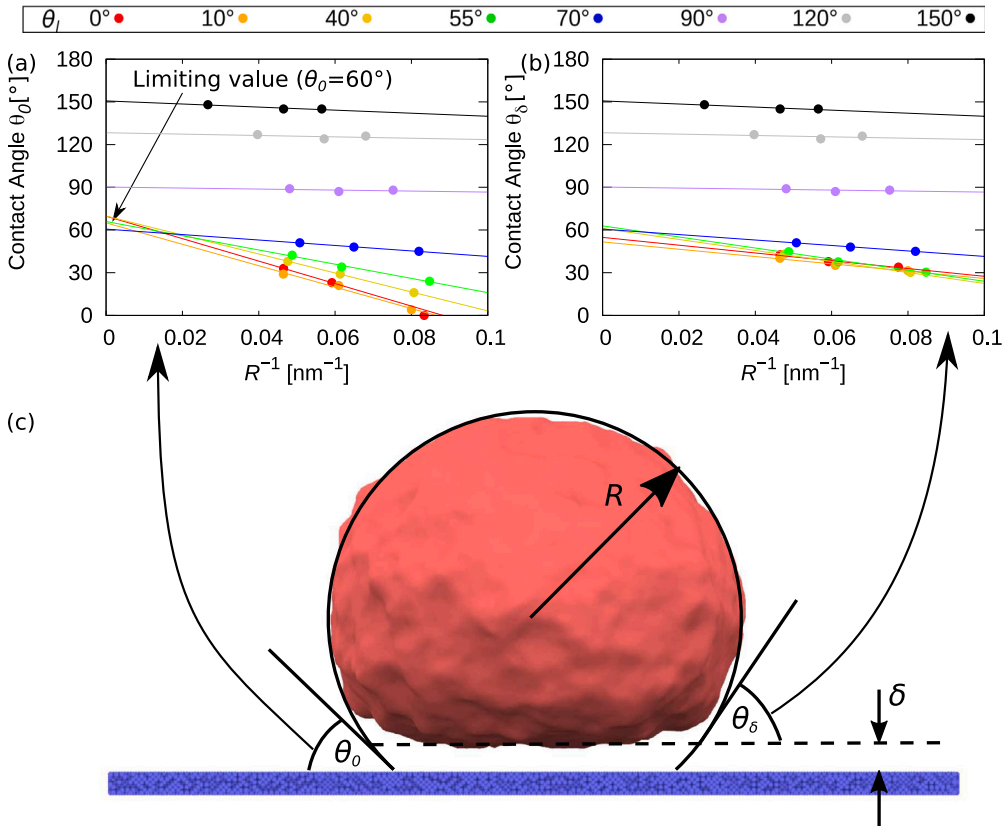

Fig. 5. Comparison of liquid contact angles measured against the (a) solid substrate θ_0 and (b) non-evaporating layer θ_δ. The solid lines represent a linear best fit, extrapolating to the macroscale limiting value of contact angle. (c) Schematic highlighting the difference between the two measurements. Note the separation of the bubble from the surface by a distance of δ due to the non-evaporating layer.

$$\gamma_{sf} - \gamma_{s0} = \int_{y_{sf}}^{y_f} (\tau_N - \tau_T) dy. \tag{20}$$

In the cases where a NEL forms, the solid-vapour interface becomes a solid-NEL-vapour interface, with a notable effect on the resulting interfacial stress. Fig. 6(a) shows how the cumulative stress changes with distance from the wall for both the $\theta_l = 70°$ and $\theta_l = 10°$ cases. We can see for the $\theta_l = 10°$ case that there is a noticeable effect from layering of molecules near the surface for both the solid-liquid and solid-vapour measurements. There is a slight offset in the location of these peaks between the solid-liquid and solid-vapour curves. This is due to the difference in far field pressure in the bulk liquid and inside the vapour bubble caused by the Laplace pressure. For $\theta_l = 70°$, the layering is only visible in the liquid. As there is no NEL, there is no layering observed in the solid-vapour cumulative stress profile. Thus the presence of the NEL significantly affects the interfacial stresses, which in turn must influence the contact angle, which we will demonstrate next. By measuring the liquid-vapour, solid-liquid, and solid-vapour interfacial stresses, γ_{lv}, γ_{sl}, and γ_{sv} respectively, we can predict the resulting contact angle using Young's equation:

$$\cos\theta_Y = \frac{\gamma_{sl} - \gamma_{sv}}{\gamma_{lv}}. \tag{21}$$

Fig. 6(b) compares the angle predicted by Young's equation (Eq. (21)) with the geometrically measured angles from our MD simulations (shown in Fig. 5(b)). We see good agreement between the predicted Young's angle θ_Y and the measured NEL-based contact angle θ_δ across the full range of wettabilities. This confirms that the NEL is responsible for the fixed θ_δ when $\theta_l < 70°$.

Formation of NEL: There remains the second question about why and when the NEL forms. To answer this, we develop a criterion based on the potential energy barrier that a molecule would need to overcome in order to evaporate from the surface into the bubble. The potential barrier consists of the attractive potential from the wall (PE_{wall}) as well as from the pressure in the vapour (PE_{vapour}), effectively pushing molecules towards the surface. We hypothesise that if the kinetic energy (KE) of the molecules is less than the potential barrier, the molecules lack sufficient energy to escape from the potential energy well of the surface and the NEL forms. Otherwise, the NEL does not form. We can then express this NEL formation criterion as:

$$KE - PE_{wall} - PE_{vapour} < 0. \tag{22}$$

This is similar to the *PK norm* measurement proposed by Chen et al. [31], who considered the local potential and kinetic energy to predict the location of bubble nucleation sites. Comparing the value of this criterion to our contact angle observations in Fig. 6(b), we can see good agreement with our simulation results. The change in sign of our NEL criterion, expected to occur when the potential barrier exceeds the available kinetic energy, occurs exactly when the NEL forms ($\theta_l \approx 70°$) and the bubble contact angle becomes independent of wettability. This provides additional evidence that the formation of the NEL is responsible for the disparities between the different contact angle measurements.

We can thus clearly see that the presence of the NEL causes the liquid-side contact angle of the vapour bubble θ_δ to deviate from predictions of a droplet analysis. When the bubble growth data is compared to the HIT theory using the measured contact angles from bubble simulations (i.e. θ_δ, Fig. 7), rather than the values obtained from droplet simulations (i.e. θ_l, Fig. 4 (a)), we see significantly improved agreement in the lyophilic regime. This indicates that while using droplet contact angles is useful for non-dimensionalising the wettability, they are not appropriate for analysing bubble systems when the NEL is present.

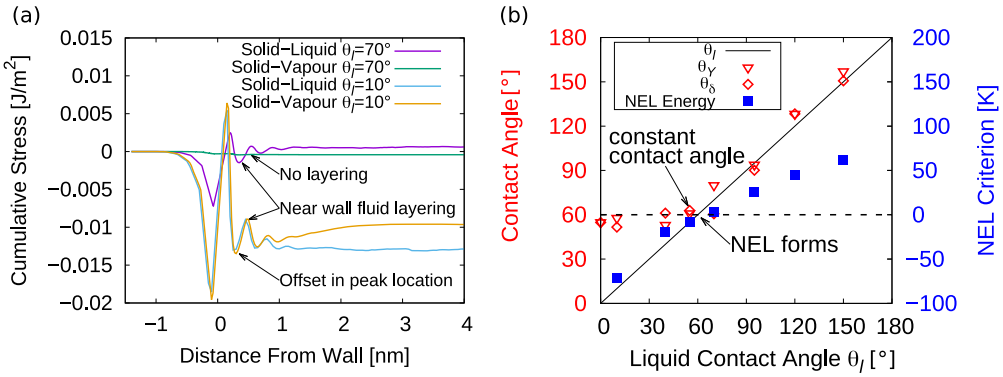

Fig. 6. (a) Interfacial stress measurements of the solid-liquid and solid-vapour interfaces for liquid contact angles of 10° and 70°. (b) Liquid contact angles predicted by Young's equation θ_Y compared to those measured from MD simulations θ_δ. The predicted angle reaches a constant value as the NEL formation criterion changes sign.

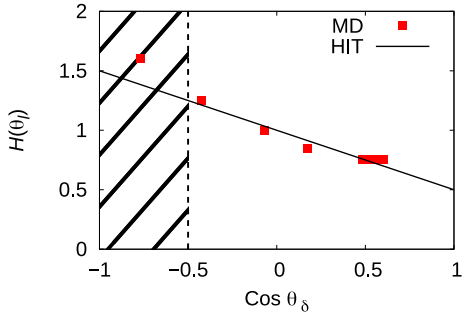

Fig. 7. Measured heterogeneous scaling factors from MD simulations compared to the HIT model predictions with measured liquid contact angle θ_δ. The hatched region where $\cos\theta_\delta < -0.5$ indicates where the model predictions do not hold in the lyophobic regime (further details in the SI). The grouping of points around $\cos\theta_\delta = 0.5$ is due to the NEL formation.

5. Conclusions

We develop a new heterogeneous inertio-thermal (HIT) model by extending our previously published homogeneous inertio-thermal model to account for the changes to diffuse heat transfer in the liquid surrounding a bubble growing on a solid surface. The model scales the bubble surface area and volume terms in the interfacial energy balance to that of an equivalent spherical cap. Additionally, the available thermal energy is scaled to be contained in a spherical cap around the bubble rather than the spherical sector that the equivalent homogeneous bubble would have available.

Three distinct regimes of bubble growth are identified. For the neutral wetting regime ($-0.5 < \cos\theta_l < 0.5$), we see excellent agreement of the HIT model predictions with MD results, with an increased growth rate observed for less wetting fluids and a decreased growth rate for more wetting fluids. In the lyophobic regime ($\cos\theta_l < -0.5$), the inertia of the system can no longer be well described by the spherical symmetry of the Rayleigh–Plesset equation and therefore cannot be accurately modelled. In the other extreme, in the lyophilic regime ($\cos\theta_l > 0.5$), a non-evaporating layer (NEL) of adsorbed molecules forms on the surface underneath the bubble. The NEL substantially alters the interfacial stress balance at the contact line, causing the measured liquid-side contact angle of the bubble θ_δ to differ from the liquid contact angle measured for a droplet i.e. $\theta_\delta \neq \theta_l$. We show that when the NEL forms, the correct bubble growth dynamics can still be obtained if the liquid contact angle measured from the top of the NEL θ_δ is used instead of the value obtained from droplet measurements θ_l in the HIT model.

This improved understanding of heterogeneous bubble growth will lead to an improved performance of bubble technologies. In particular, we now have a better understanding of the role the surface plays on the thermal diffusion in the bulk liquid, which may provide additional insights for the design of phase change thermal management systems. The effect of surface adsorption in forming the non-evaporating layer has been shown to significantly alter the geometry of vapour bubbles. It has yet to be determined what effect this has on the interfacial heat transfer as the bubble grows, providing a promising avenue for future research.

Declaration of competing interest

The authors declare that they have no known competing financial interests or personal relationships that could have appeared to influence the work reported in this paper.

Data availability

The data that support the findings of this study are openly available in the Edinburgh DataShare repository at https://doi.org/10.7488/ds/7511.

Acknowledgements

This work was supported in the UK by the Engineering and Physical Sciences Research Council (EPSRC) under Grant Nos. EP/N016602/1, EP/R007438/1, and EP/V012002/1. All MD simulations were run on ARCHER2, the UK's national supercomputing service, funded by an EPSRC/ARCHER2 Pioneer Project. Duncan Dockar is supported by the Royal Academy of Engineering under the Research Fellowship programme.

Appendix A. Supplementary material

Supplementary material related to this article can be found online at https://doi.org/10.1016/j.ijheatmasstransfer.2023.124657.

References

[1] A. Prosperetti, Vapor bubbles, Annu. Rev. Fluid Mech. 49 (2017) 221–269.
[2] C.E. Brennen, Cavitation and Bubble Dynamics, Cambridge University Press, 2013.
[3] V. Carey, Liquid Vapor Phase Change Phenomena: An Introduction to the Thermophysics of Vaporization and Condensation Processes in Heat Transfer Equipment, second edition, Taylor and Francis, 2018.
[4] L. Rayleigh, On the pressure developed in a liquid during the collapse of a spherical cavity, Lond. Edinb. Dublin Philos. Mag. J. Sci. 34 (1917) 94–98.
[5] M.S. Plesset, S.A. Zwick, The growth of vapor bubbles in superheated liquids, J. Appl. Phys. 25 (1954) 493–500.
[6] A. Prosperetti, M.S. Plesset, Vapour-bubble growth in a superheated liquid, J. Fluid Mech. 85 (1978) 349–368.
[7] A. Prosperetti, A generalization of the Rayleigh-Plesset equation of bubble dynamics, Phys. Fluids 25 (1982) 409.

[8] B.B. Mikic, W.M. Rohsenow, P. Griffith, On bubble growth rates, Int. J. Heat Mass Transf. 13 (1970) 657–666.
[9] H.S. Lee, H. Merte, Spherical vapor bubble growth in uniformly superheated liquids, Int. J. Heat Mass Transf. 39 (1996) 2427–2447.
[10] A.J. Robinson, R.L. Judd, The dynamics of spherical bubble growth, Int. J. Heat Mass Transf. (2004).
[11] P. Sullivan, D. Dockar, M.K. Borg, R. Enright, R. Pillai, Inertio-thermal vapour bubble growth, J. Fluid Mech. 948 (2022) 55.
[12] D. Kaschiev, Nucleation: Basic Theory with Applications, Butterworth Heinemann, 2000.
[13] O.R. Enríquez, C. Sun, D. Lohse, A. Prosperetti, D. Van Der Meer, The quasi-static growth of CO2 bubbles, J. Fluid Mech. 741 (2014) 1.
[14] M.G. Cooper, A.J. Lloyd, The microlayer in nucleate pool boiling, Int. J. Heat Mass Transf. 12 (1969) 895–913.
[15] S.J. van Stralen, R. Cole, W.M. Sluyter, M.S. Sohal, Bubble growth rates in nucleate boiling of water at subatmospheric pressures, Int. J. Heat Mass Transf. 18 (1975) 655–669.
[16] H.T. Phan, N. Caney, P. Marty, S. Colasson, J. Gavillet, A model to predict the effect of contact angle on the bubble departure diameter during heterogeneous boiling, Int. Commun. Heat Mass Transf. 37 (2010) 964–969.
[17] H.C. Lee, B.D. Oh, S.W. Bae, M.H. Kim, Single bubble growth in saturated pool boiling on a constant wall temperature surface, Int. J. Multiph. Flow 29 (2003) 1857–1874.
[18] F.J. Lesage, S. Siedel, J.S. Cotton, A.J. Robinson, A mathematical model for predicting bubble growth for low Bond and Jakob number nucleate boiling, Chem. Eng. Sci. 112 (2014) 35–46.
[19] X. Chang, H. Huang, Y.P. Cheng, X.Y. Lu, Lattice Boltzmann study of pool boiling heat transfer enhancement on structured surfaces, Int. J. Heat Mass Transf. 139 (2019) 588–599.
[20] Z. Zhao, J. Zhang, D. Jia, K. Zhao, X. Zhang, P. Jiang, Thermal performance analysis of pool boiling on an enhanced surface modified by the combination of microstructures and wetting properties, Appl. Therm. Eng. 117 (2017) 417–426.
[21] K.H. Ardron, G. Giustini, On the wetting behavior of surfaces in boiling, Phys. Fluids 33 (2021).
[22] S.C. Maroo, J.N. Chung, Fundamental roles of nonevaporating film and ultrahigh heat flux associated with nanoscale meniscus evaporation in nucleate boiling, J. Heat Transf. (2013).
[23] J.N. Chung, T. Chen, S.C. Maroo, A review of recent progress on nano/micro scale nucleate boiling fundamentals, Front. Heat Mass Transf. 2 (2011).
[24] M. Gallo, F. Magaletti, C.M. Casciola, Heterogeneous bubble nucleation dynamics, J. Fluid Mech. 906 (2021) 20.
[25] S.C. Maroo, J.N. Chung, Molecular dynamic simulation of platinum heater and associated nano-scale liquid argon film evaporation and colloidal adsorption characteristics, J. Colloid Interface Sci. 328 (2008) 134–146.
[26] S. Datta, R. Pillai, M.K. Borg, K. Sefiane, Acoustothermal nucleation of surface nanobubbles, Nano Lett. 21 (2021) 1267–1273.
[27] L. Scriven, On the dynamics of phase growth, Chem. Eng. Sci. 10 (1959) 1–13.
[28] J. Israelachvili, Intermolecular and Surface Forces, 2011.
[29] P.-G. de Gennes, F. Brochard-Wyart, D. Quéré, Capillarity and Wetting Phenomena, 2004.
[30] S. Plimpton, Fast parallel algorithms for short-range molecular dynamics, J. Comput. Phys. 117 (1995) 1–19.
[31] Y.J. Chen, B. Yu, Y. Zou, B.N. Chen, W.Q. Tao, Molecular dynamics studies of bubble nucleation on a grooved substrate, Int. J. Heat Mass Transf. 158 (2020).
[32] G. Nagayama, P. Cheng, Effects of interface wettability on microscale flow by molecular dynamics simulation, Int. J. Heat Mass Transf. 47 (2004) 501–513.
[33] X.D. Din, E.E. Michaelides, Transport processes of water and protons through micropores, AIChE J. 44 (1998) 35–47.
[34] J.L. Barrat, L. Bocquet, Large slip effect at a nonwetting fluid-solid interface, Phys. Rev. Lett. 82 (1999) 4671–4674.
[35] L. Zhang, J. Xu, G. Liu, J. Lei, Nucleate boiling on nanostructured surfaces using molecular dynamics simulations, Int. J. Therm. Sci. 152 (2020) 106325.
[36] L. Martínez, R. Andrade, E.G. Birgin, J.M. Martínez, Packmol: a package for building initial configurations for molecular dynamics simulations, J. Comput. Chem. 30 (2009) 2157–2164.
[37] L.C. Malan, A.G. Malan, S. Zaleski, P.G. Rousseau, A geometric VOF method for interface resolved phase change and conservative thermal energy advection, J. Comput. Phys. 426 (2021) 109920.
[38] J.H. Irving, J.G. Kirkwood, The statistical mechanical theory of transport processes. IV. The equations of hydrodynamics, J. Chem. Phys. 18 (1950) 817–829.
[39] Y. Yamaguchi, H. Kusudo, D. Surblys, T. Omori, G. Kikugawa, Interpretation of Young's equation for a liquid droplet on a flat and smooth solid surface: mechanical and thermodynamic routes with a simple Lennard-Jones liquid, J. Chem. Phys. 150 (2019).
[40] S. Nishida, D. Surblys, Y. Yamaguchi, K. Kuroda, M. Kagawa, T. Nakajima, H. Fujimura, Molecular dynamics analysis of multiphase interfaces based on in situ extraction of the pressure distribution of a liquid droplet on a solid surface, J. Chem. Phys. 140 (2014) 074707.